

Sharmila Dorbala

5.1 Background

Systemic amyloidoses are a group of protein misfolding disorders that are typified by the extracellular deposition of insoluble, non-branching, amyloid fibrils with a common beta-pleated sheet structure [1, 2]. Misfolding of over 25 unique precursor proteins can cause amyloidosis. Amyloid fibrils from the precursor proteins—immunoglobulin light chains (primary or AL) and the transthyretin protein (TTR)—usually involve the heart. AL amyloidosis is a plasma cell dyscrasia with an overproduction of abnormal kappa or lambda immunoglobulin light chains that aggregate into AL fibrils. ATTR amyloidosis, however, results from aggregation of either native (senile systemic amyloidosis) or variant TTR protein (familial amyloidosis) produced by the liver of individuals with mutations of the TTR gene (>100 single nucleotide polymorphisms and 80 confirmed mutations described) [3]. Senile systemic amyloidosis affects older individuals (>70 years) and almost always affects the heart. Variant TTR protein can cause familial amyloid cardiomyopathy, familial amyloid neuropathy, or mixed disease (cardiomyopathy and neuropathy) and younger individuals (fourth decade of life or later) may manifest clinical symptoms [4].

Most individuals with cardiac amyloidosis present with heart failure, from diastolic or systolic dysfunction, as their first symptom. But, due to the multitude of symptoms from systemic disease—involvement of the gastrointestinal tract,

S. Dorbala, MD, MPH, FACC

Noninvasive Cardiovascular Imaging Program, Departments of Radiology and Medicine (Cardiology), Brigham and Women's Hospital, Harvard University, Boston, MA, USA

Cardiac Amyloidosis Program, Department of Medicine, Brigham and Women's Hospital, Harvard Medical School Boston, MA, USA

Brigham and Women's Hospital, Harvard Medical School, Boston, MA, USA

e-mail: SDORBALA@PARTNERS.ORG

peripheral and autonomic nervous system, heart, or kidneys—recognition of amyloidosis (and cardiac involvement) is typically delayed. Also, the clinical features of AL and ATTR cardiac amyloidosis are so similar that the two entities cannot be distinguished from one another on clinical grounds alone. Their prognosis and management, however, are vastly different [5, 6]. Individuals with AL cardiac amyloidosis, if untreated, have a median survival of 18–24 months; [1] highly effective AL chemotherapy directed against the clonal plasma cells, with or without stem cell transplantation, is poorly tolerated by individuals with cardiac involvement [7]. On the other hand, until recently, no specific therapies were available for ATTR amyloidosis. Currently, several novel agents (tafamidis or difunisal) are under development to stabilize the tetrameric form of TTR and prevent it from becoming a monomer which is more prone to aggregate [3]. Other treatment approaches include antisense oligonucleotides to silence the TTR gene (Alnylam compound or Isis pharmaceuticals compound), small interfering RNA molecules to reduce the production of the mutant TTR from the liver, or agents to dissolve the amyloid fibrils from the various organs (doxycycline/TUDCA) [3]. Liver transplantation removes the source of the variant TTR and replaces it with normal TTR and is a major treatment option in individuals with familial amyloid cardiomyopathy [3]. ATTR amyloidosis, however, can recur following liver transplantation [8]. Due to the distinct clinical course and treatment options for AL and ATTR amyloidosis, early diagnosis of cardiac amyloidosis as well as typing of AL or ATTR disease are critical [9].

5.2 Diagnosis of Cardiac Amyloidosis

Cardiac amyloidosis is usually suspected clinically and evaluated by a variety of diagnostic tests. A 12-lead ECG and 2D transthoracic echocardiography are common first tests; they are followed by advanced imaging with cardiac magnetic resonance imaging or radionuclide imaging when clinical suspicion for cardiac amyloidosis is high. Each of these tests provides insights into specific pathophysiological processes in the heart of individuals with amyloidosis (Table 5.1).

The most definitive diagnosis, however, is by endomyocardial biopsy. After the amyloid deposits are identified on histology (Congo red or sulfated Alcian blue staining), the precursor protein for the fibrils is identified by immunohistochemistry staining for kappa and lambda light chains or transthyretin. Transthyretin protein is further analyzed to distinguish variant TTR from wild-type TTR. But, none of these tests is diagnostic on its own, including endomyocardial biopsy which may rarely be false negative due to sampling error [9]. The information obtained from each of these tests is integrated with clinical data to diagnose amyloidosis, to plan management, and to screen family members of individuals with genetic forms of amyloidosis.

Table 5.1 Typical imaging features in cardiac amyloidosis

ECG	Low voltage: <5 mm in limb leads and <10 mm in the chest leads
Echocardiogram	Thick LV and RV myocardium
	Sparkling/granular appearance
	Increased LV mass
	Small LV cavity size
	LV wall thickness-to-ECG voltage ratio
	Biatrial enlargement
	Pericardial effusions
	Restrictive filling pattern
	Mitral E/A TDI
	Pulmonary venous inflow (S > D) RVTDI
	LV longitudinal systolic strain with apical sparing—apical-to-basal strain ratio >2.1
CMR	Above structural features Late gadolinium enhancement—diffuse, patchy, subendocardial LGE in the left ventricle, atria, and the right ventricle Expanded ECV Nulling of myocardial signal prior to blood pool signal on T1 scout
Radionuclide imaging	Tc-99m DPD uptake—ATTR amyloidosis Tc-99m PYP uptake—ATTR amyloidosis C-11 PiB uptake—AL and ATTR amyloidosis F-18 florbetapir uptake—AL and ATTR amyloidosis

LV left ventricle, RV right ventricle, ECG electrocardiogram, TDI tissue Doppler imaging, LGE late gadolinium enhancement, ECV extracellular volume, ATTR transthyretin amyloidosis, AL light chain amyloidosis, DPD = 3,3-diphosphono-1,2-propanodicarboxylic acid, PYP = pyrophosphate; PiB = Pittsburgh B compound.

5.2.1 ECG

A classic finding of cardiac amyloidosis is the paradox of a low-voltage ECG (<0.1 mV in all the chest leads or <0.05 mV in all the standard limb leads) in individuals with increased LV wall thickening (Fig. 5.1). Unfortunately, this predicts amyloidosis in only 56 % of individuals with cardiac amyloidosis [10]. These low-voltage ECG patterns are most common in individuals with AL rather than ATTR amyloidosis [6, 11]. Adding to this enigma, individuals with amyloidosis may manifest normal ECG voltage or even high ECG voltage meeting criteria for LVH (especially with senile systemic amyloidosis and coexistent hypertension) [12]. The precise reasons for the low-voltage ECG are not known, but, myocyte atrophy and/or local myotoxicity from circulating AL and amyloid fibril component interactions are possible causal factors [6]. Other significant ECG findings in cardiac amyloidosis patients include pseudoinfarction patterns (66–69 %), atrial fibrillation (5–27 %),

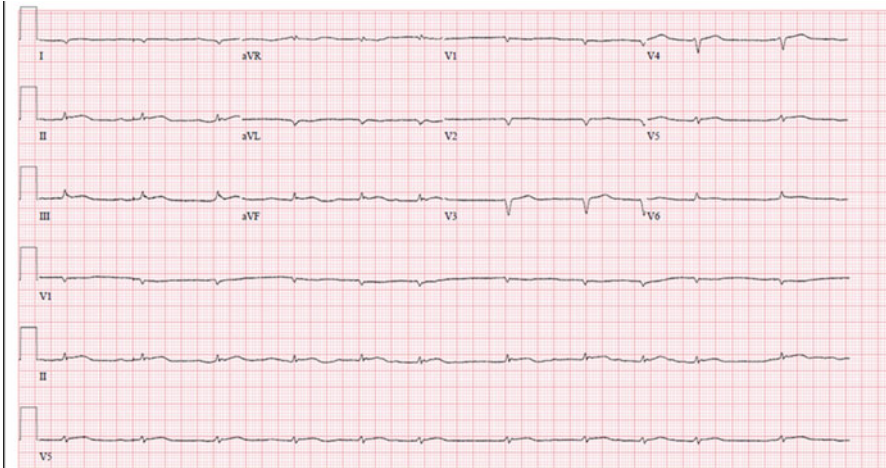


Fig. 5.1 Typical ECG in cardiac amyloidosis. A 60-year-old man with AL cardiac amyloidosis has atrial fibrillation, low-voltage ECG in precordial and limb leads, and pseudo Q-waves

first-degree AV block, RBBB, or LBBB (4–33 %) [10, 13, 14]. A 12-lead ECG, though an appropriate first step, is not sufficiently diagnostic on its own. Further evaluation with advanced imaging is often necessary.

5.2.2 Echocardiography

Echocardiography, in cardiac amyloidosis, is fundamental to establish the diagnosis, to define the magnitude of myocardial dysfunction, to guide management, and to define prognosis [15–24]. A comprehensive advanced transthoracic 2D echocardiogram study for cardiac amyloidosis includes assessment of (1) cardiac structure by 2D imaging (Fig. 5.2), (2) valve function by color and spectral Doppler imaging, (3) myocardial relaxation by tissue Doppler imaging of the right and left ventricle, and (4) myocardial deformation by 2D tissue Doppler or speckle tracking longitudinal and radial strain imaging of the left and the right ventricles. Transesophageal echocardiography may be frequently performed, prior to cardioversion, in individuals with atrial fibrillation which is common in cardiac amyloidosis.

The classic 2D echocardiographic features of sparkling myocardium and increased left ventricular (LV) wall thickness (Fig. 5.2a, b) typically indicate advanced myocardial infiltration with amyloid. Unlike left ventricular myocardial hypertrophy from increased afterload (hypertensive heart disease or aortic stenosis), the increased wall thickness in amyloidosis represents amyloid deposits, usually parallels disease burden, and is associated with low-voltage ECG [10]. The sparkling myocardial appearance, present in about 25 % of individuals [10], is not specific for amyloidosis and may be seen with other forms of hypertrophic diseases. Increased LV wall thickness (>12 mm), decreased LV end-diastolic and end-systolic

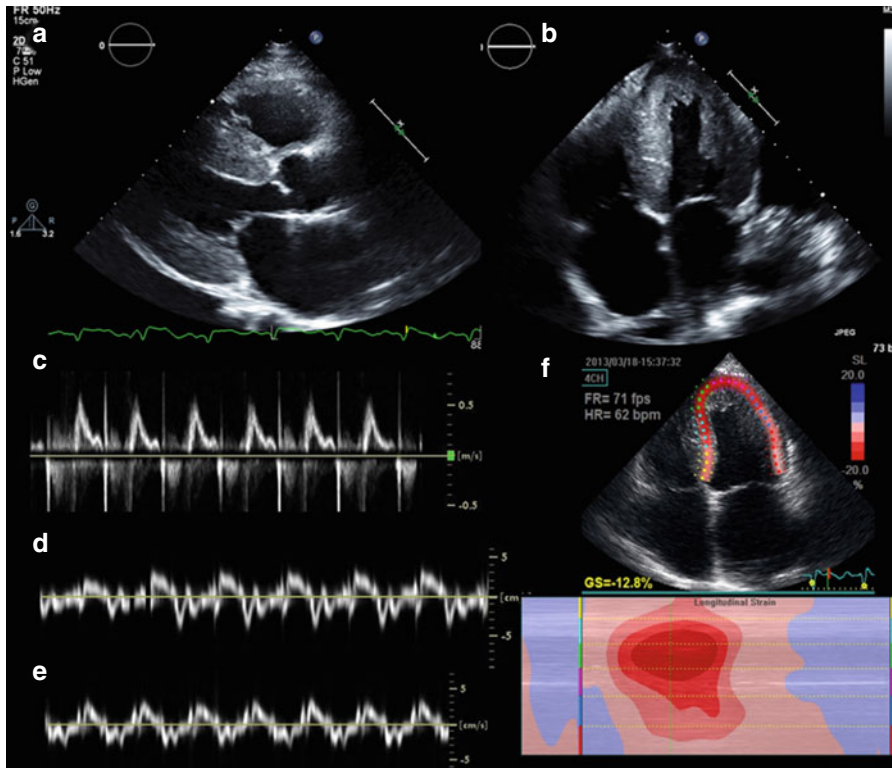


Fig. 5.2 Typical echocardiographic features of cardiac amyloidosis. Increased left ventricular wall thickness with sparkling myocardium on parasternal long-axis (a), apical four-chamber views (b) and restrictive filling pattern on the mitral inflow (c), and mitral annular tissue Doppler imaging (TDI, (d) septal, (e) lateral). Panel (f) shows typical longitudinal systolic strain pattern with apical sparing (red in the center of the bulls eye plot represents preserved apical strain)

volumes, biatrial enlargement, right ventricular (RV) hypertrophy, pericardial effusions, thickening of the interatrial septum (a specific feature) [24], and increased atrioventricular valve thickening characterize cardiac amyloidosis [6, 10, 25].

Imaging of myocardial relaxation by spectral and tissue Doppler imaging demonstrates classic features of restrictive heart disease (Fig. 5.2c–e): E/A reversal, short deceleration time, high E-wave velocity, and reduced pulmonary venous systolic velocity [26]. Tissue Doppler imaging as well as pulmonary inflow parameters are more sensitive than the mitral inflow parameters to identify earlier stages of restriction [15]. While the mitral early diastolic tissue Doppler velocities (e') are reduced early, before onset of overt congestive heart failure (CHF), peak S-wave velocity on pulmonary venous flow and mitral inflow E-wave deceleration time are later manifestations and are seen in individuals with overt CHF [20]. Objective evidence of abnormalities in diastolic filling portends worse outcomes [27], incremental to LV wall thickening and fractional shortening [17].

Left ventricular myocardial deformation, global longitudinal strain, using 2D tissue Doppler or speckle tracking, is a sensitive and early marker of myocardial systolic dysfunction. Abnormalities in longitudinal strain, with a classic pattern of apical sparing on 2D (Fig. 5.2f) [20] or 3D strain imaging [28], may precede an overt decline of LV ejection fraction. Although the ratio of longitudinal strain at the apex to base (>2.1) may distinguish amyloid heart disease from other forms of LV hypertrophy, there is significant overlap [28, 29].

The right ventricle is almost universally thickened in cardiac amyloidosis. Reductions in RV longitudinal strain as well as tricuspid annular plane systolic excursion (TAPSE) are early markers of cardiac amyloidosis [27, 30] and independent predictors of cardiac death [27].

Although echocardiography is almost invariably the initial test in most individuals with symptoms suggestive of cardiac amyloidosis, it remains insensitive to detect early disease. Also, echocardiography cannot definitively diagnose cardiac amyloidosis from other hypertrophic heart diseases and cannot distinguish AL from ATTR amyloidosis. When the echocardiogram shows classic features, in individuals with biopsy-proven systemic AL amyloidosis, cardiac amyloidosis is diagnosed, and an endomyocardial biopsy is spared. On the other hand, if echocardiogram is classic and systemic, AL amyloidosis is excluded by serum-free light chain assay and serum/urine immunofixation studies, ATTR amyloidosis is possible. Prior to endomyocardial biopsy to confirm ATTR amyloidosis, advanced imaging with cardiac MRI or radionuclide imaging may be performed [9].

5.2.3 Cardiac Magnetic Resonance Imaging

Cardiac magnetic resonance imaging (CMR) is a powerful method to image cardiac structure, function, and amyloid deposition. Clinically, CMR is typically considered in individuals with echocardiograms that are suspicious but not typical for amyloidosis or in individuals with high clinical suspicion, irrespective of echocardiogram results (gene-positive individuals with symptoms or at the age when disease onset is expected). Standard CMR sequences for cardiac amyloidosis include (1) cine images in the standard long-axis and short-axis views to study cardiac structure, systolic function, calculate LV wall thickness and mass; (2) late gadolinium enhancement imaging (about 5 min after injection of gadolinium) in axial, short-, and long-axis views; (3) optimal myocardial inversion time is assessed about 4 min after injection of gadolinium (0.05 mmol/kg of gadolinium at 3 cc/s) to identify specific patterns of myocardial nulling in amyloid as opposed to left ventricular myocardial hypertrophy; and (4) T1 mapping native (precontrast) and post-gadolinium contrast T1 mapping to calculate extracellular volume (ECV).

CMR, with excellent spatial resolution, can characterize the classic phenotypic changes of cardiac amyloidosis, including increased LV and RV wall thickness, myocardial mass, biatrial enlargement, pericardial effusions, and pleural effusions (Fig. 5.3a, b) [31–34].

Cardiac amyloid deposits can substantially alter myocardial tissue characteristics. Intravenous gadolinium administration markedly reduces the myocardial longitudinal relaxation times (T-1) [32], corresponding to histological distribution of amyloid deposits, with significantly lower T-1 times in the subendocardium compared to the subepicardium [32]. Also, the myocardial T-1 times correlated with myocardial amyloid mass as assessed by left ventricular mass and parameters of diastolic dysfunction [32].

Late gadolinium enhancement (LGE), especially in the subendocardial region, is common (80–90 %) in biopsy-proven advanced cardiac amyloidosis [32–35]. Several patterns of late gadolinium enhancement (diffuse or focal subendocardial, focal or diffuse myocardial patterns) are described, but LGE of the papillary muscle [34] and atria is a distinctive feature of cardiac amyloidosis (Fig. 5.3c, d) [33, 35]. Of note, in cardiac amyloidosis, identifying an appropriate nulling of the normal

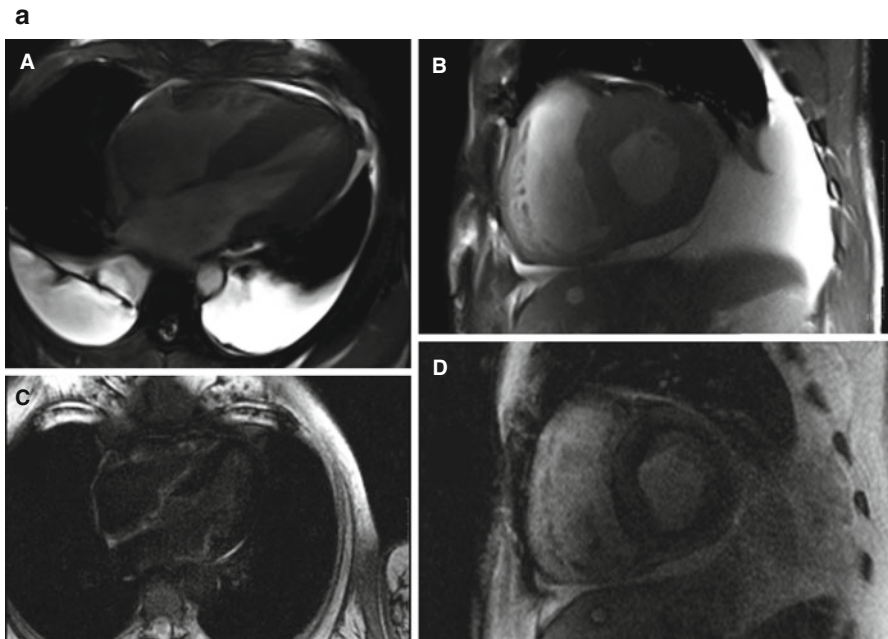


Fig. 5.3 (a) Cardiac magnetic resonance imaging features of cardiac amyloidosis. Typical features of cardiac amyloidosis on CMR are shown. Left ventricular wall thickness is increased concentrically with and small ventricular cavity and bilateral pleural effusions [A (apical four-chamber view) and B (mid-ventricular short-axis view)]. The late gadolinium enhancement (LGE) images in C (apical four-chamber view) show subendocardial LGE in the right ventricle and the right atrium (different patient than in A); D demonstrates diffuse LGE of the left ventricle (same patient as in A). Typical TI (inversion time) scout images in cardiac amyloidosis are shown in panel B (reproduced with permission from Ref. [35]). (b) The images demonstrate that, in contrast to individuals with hypertensive left ventricular hypertrophy in whom the blood pool signal nulls prior to the myocardial signal (*top panel*), in individuals with cardiac amyloidosis (*bottom panel*), the myocardial signal nulls prior to the blood pool signal consistent with diffuse late gadolinium enhancement

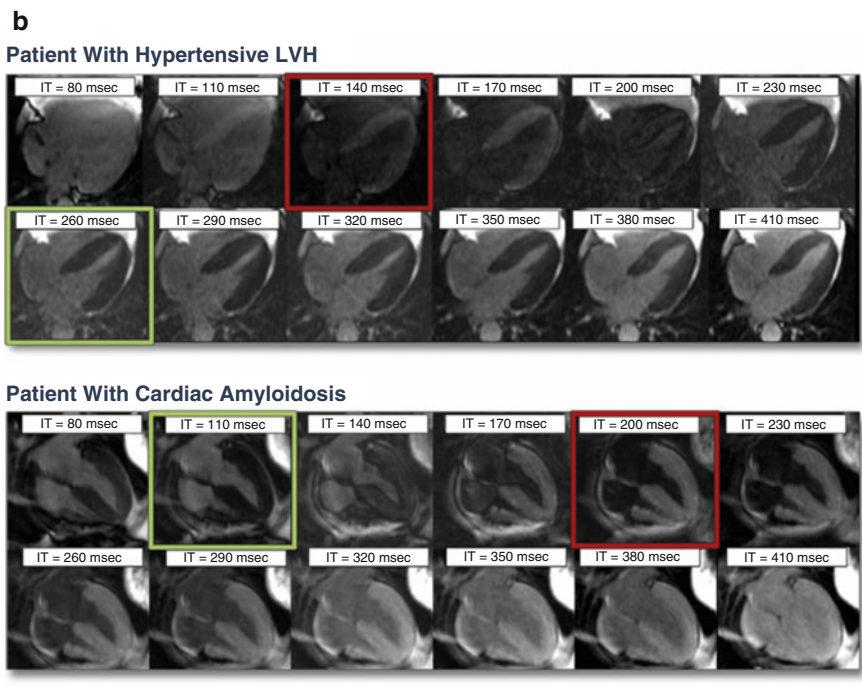


Fig. 5.3 (continued)

myocardium can be a challenge and may provide a false-negative result if an incorrect inversion time (TI inversion time) is used. However, when imaged appropriately, global transmural and subendocardial LGE patterns correlate with left ventricular mass index and cardiac amyloid burden on histology [33]. Furthermore, in one study of 47 patients with suspected cardiac amyloidosis, presence of LGE was predictive of worse survival [35].

Furthermore, in cardiac amyloidosis, on post-gadolinium contrast images, the myocardium nulls prior to blood pool on the TI-scout images; this unique feature distinguishes cardiac amyloidosis from hypertensive left ventricular hypertrophy (Fig. 5.4) [36].

For the TI scout, a sequence of images are obtained in the mid-ventricular short-axis view and a four-chamber view, using a breath-hold, inversion-recovery cine steady-state free precession (SSFP) pulse sequences, with sequential images of the phases of the cardiac cycle acquired at increasing time from the inversion pulse in 40 ms increments starting at 80 ms [34, 36]. The TI time where 50 % of the normal myocardium nulls prior to the blood pool has been used as the optimal TI time for obtaining the late gadolinium enhancement images [34]. A rapid visual assessment of TI time was helpful to identify cardiac amyloidosis individuals at high risk of mortality [36]. Also, 20–30 % of individuals with AL cardiac amyloidosis have renal dysfunction; a CMR technique that does not require gadolinium contrast, native T-1, is of great interest.

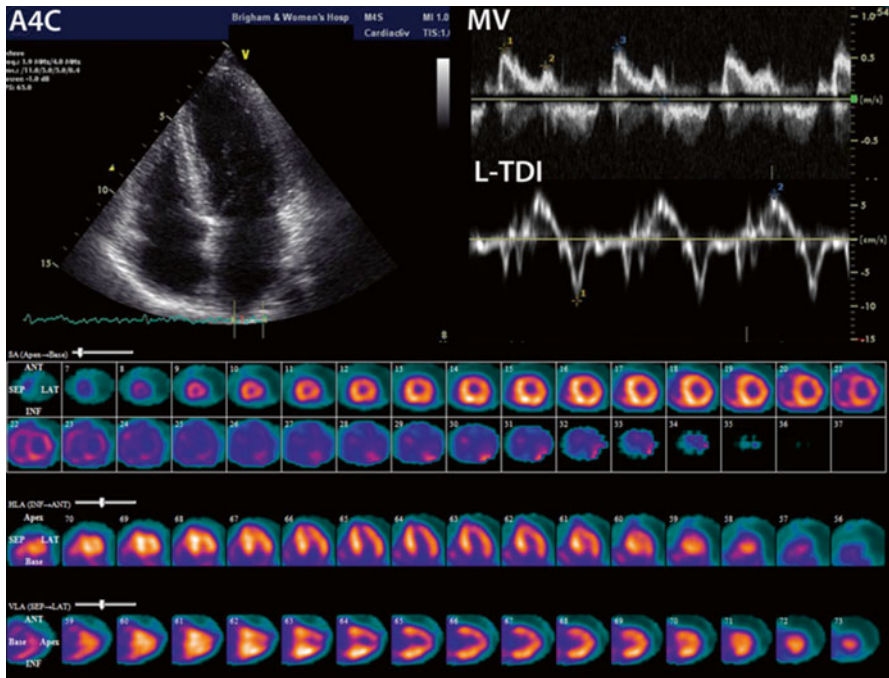


Fig. 5.4 Technetium-99m pyrophosphate imaging in familial transthyretin cardiac amyloidosis. Echocardiogram and technetium-99m pyrophosphate (PYP) images of a 55-year-old woman positive for Ala60 TTR variant and a family history of TTR amyloid cardiomyopathy and neuropathy. The echocardiogram shows relatively normal wall thickness, normal E/A ratio, but significantly impaired lateral mitral annular systolic and diastolic motion by tissue Doppler imaging (*TDI*). In the bottom panel, the Tc-99m PYP images in short axis (*top*), vertical long axis (*middle*), and horizontal long axis (*bottom*) demonstrate moderate, diffusely increased radiotracer uptake in the left and right ventricles suggesting early cardiac involvement

Native (precontrast) T-1 relaxation times were significantly increased in patients with cardiac amyloidosis compared to healthy volunteers [(AL 1140 ± 61 ms vs. healthy 958 ± 20 ms) [37] (ATTR 1097 ± 43 ms vs. healthy 967 ± 34 ms) [38]]. Individuals with AL and ATTR cardiac amyloidosis also have significantly higher T-1 compared to individuals with left ventricular hypertrophy from aortic stenosis [37] or hypertrophic cardiomyopathy [38]. In a study of patients with AL cardiac amyloidosis, increased T-1 time was observed in all patients with LGE [37]. Increased T-1 time correlated with disease burden and was linearly related to myocardial mass ($r=0.58$, $p<0.001$) and inversely related to left ventricular ejection fraction ($r=-0.57$, $p<0.001$) and diastolic function (E/E' ratio; $r=0.44$, $p=0.001$). A higher native T-1 (1,044 ms) also predicted a higher hazard of mortality (HR 5.09, 95 % CI 1.09–23.7, $p=0.04$) in patients with AL amyloidosis [39]. Despite the advantages of not using gadolinium contrast, native T-1 mapping has certain challenges: (1) it measures signal from the myocardium and the interstitial space, (2) it cannot differentiate edema from amyloid, and (3) normal reference values are not standardized and may vary by the type of scanner used [40].

Using advanced techniques, myocardial T-1 times measured by post-gadolinium contrast can quantify expanded myocardial ECV from various cardiovascular pathologies including amyloid deposits [41, 42]. Indeed, ECV is significantly expanded in cardiac amyloidosis (mean ECV 0.44 ± 0.12) compared to healthy controls (mean ECV 0.25 ± 0.02 , $p < 0.001$) [39]. Expanded ECV [41, 42] and prolonged T1 relaxation times [37] are directly related to myocardial amyloid burden; they correlate directly with LV mass [37], restrictive features (TDI “S” wave) [41, 42], elevated cardiac biomarker levels (BNP and troponin levels) [41], myocardial uptake of Tc-99m DPD (a specific radiotracer that images ATTR amyloid in the heart) [37], and inversely with left ventricular ejection fraction [37, 41]. Moreover, ECV predicted mortality after accounting for echocardiographic features of diastolic dysfunction, EF, and NT pro BNP levels (HR 4.4.1; 95 % CI 1.35–14.4, $p < 0.0001$) [39]. Although there are no data, being quantitative metrics, T1 mapping and ECV may serve as valuable tools to longitudinally assess the fate of cardiac amyloid burden in response to therapy.

CMR, however, may be limited in individuals with atrial fibrillation or claustrophobia; gadolinium-based contrast agents are contraindicated in individuals with renal dysfunction, and CMR is contraindicated in individuals with certain cardiac devices (pacemakers, ICD). When feasible, CMR plays a major role in the evaluation of individuals with suspected cardiac amyloidosis. In individuals with biopsy-proven systemic AL amyloidosis, classic CMR findings are virtually diagnostic of cardiac amyloidosis. CMR features, however, cannot definitively distinguish AL amyloidosis from ATTR amyloidosis. Therefore, when cardiac amyloidosis is suspected for the first time based on CMR findings, serum-free light chain assay and serum and urine immunofixation are recommended to exclude systemic AL amyloidosis [9]. If those evaluations are negative, to identify ATTR cardiac amyloidosis, either an endomyocardial biopsy or a radionuclide study using technetium-99m pyrophosphate (Tc-99m PYP) is the next step.

5.2.4 Radionuclide Imaging of Cardiac Amyloidosis

Targeted radionuclide imaging of amyloidosis is a robust method to image cardiac amyloid deposition. Radionuclide imaging is typically considered for the diagnosis of amyloidosis in individuals with a high clinical suspicion for ATTR cardiac amyloidosis. More recently, it is also being used for identifying ATTR amyloidosis when echocardiography or CMR are highly suggestive of amyloidosis, but endomyocardial biopsy is not planned, as in elderly individuals with senile systemic amyloidosis. Radionuclide imaging of cardiac amyloidosis is possible with (1) bone imaging SPECT agents (technetium-99m (Tc-99m) pyrophosphate/Tc-99m 3,3-diphosphono-1,2-propanodicarboxylic acid (DPD)), (2) neuronal imaging agents (I-123 meta iodo benzyl guanidine, mIBG), (3) amyloid-binding SPECT agents (I-123 serum amyloid protein-SAP, Tc-99m aprotinin), and (4) amyloid-binding PET agents (C-11 Pittsburgh B compound, PiB, F-18 florbetapir).

5.2.5 Bone Imaging Agents

Radionuclide imaging with Tc-99m PYP or Tc-99m DPD has been used since the 1980s [43], but has recently reemerged as a dominant method for cardiac ATTR amyloid imaging. Extensive literature supports the utility of Tc-99m DPD and PYP imaging to diagnose cardiac amyloidosis [44–46] and to stratify risk of major adverse cardiac events (MACE). The precise mechanism of myocardial uptake of bone imaging agents is not known, but a calcium-mediated mechanism of uptake has been proposed [46]. Tc-99m PYP or DPD (15–20 mCi) is administered intravenously followed by planar or SPECT imaging (preferred) 2.5 h later (Table 5.2). The myocardial radiotracer uptake is semiquantitatively interpreted in relation to sternal uptake into four grades: 0=no uptake, 1=less than sternal uptake, 2=equal to sternal uptake, and 3=greater than sternal uptake (attenuation of bone uptake) [44]. When available, quantitation on SPECT/CT images may be preferable to avoid overlap from bone radiotracer uptake [47].

Tc-99m PYP and DPD are highly sensitive (>90 %) to diagnose cardiac ATTR amyloidosis [47]. Further, two studies demonstrated that Tc-99m DPD [44] and Tc-99m PYP [46] were able to noninvasively differentiate between AL and TTR amyloidosis, with all TTR patients showing DPD/PYP uptake and none of the AL patients showing DPD/PYP uptake. A heart-to-contralateral lung Tc-99m PYP ratio of 1.5 distinguished AL from ATTR cardiac amyloidosis with 97 % sensitivity and 100 % specificity [46]. In another study, however, low-level Tc-99m DPD uptake was detected in about a third of individuals with AL amyloidosis, but none with significant uptake [45]. Hutt et al. [47] demonstrated significant uptake of Tc-99m DPD in the heart and in the muscles of individuals with wild-type and V122I ATTR patients. These authors suggest that if Tc-99m DPD uptake is \geq grade 2 with typical soft tissue, the scan is diagnostic for ATTR cardiac amyloidosis, and a confirmatory endomyocardial biopsy may be avoided [47]. Finally, Tc-99m DPD imaging may identify early cardiac amyloidosis in gene-positive individuals without apparent structural cardiac changes by echocardiography (Fig. 5.5).

Table 5.2 Tc-99m PYP study protocol for suspected cardiac transthyretin amyloidosis

Tc-99m PYP is injected intravenously (20–25 mCi) and 20 min imaging is performed after 2.5 h
Planar or chest SPECT (preferred) imaging may be performed
Normal individuals have no myocardial uptake and no blood pool activity at 2.5 h
Individuals with TTR amyloidosis demonstrate significant, biventricular, diffuse myocardial uptake
Myocardial radiotracer uptake is graded on a 0–3 scale <ul style="list-style-type: none"> 0=no myocardial uptake 1 < bone uptake 2 = bone uptake and 3 > bone uptake
Heart-to-contralateral lung ratio can be computed
SPECT single-photon emission computed tomography

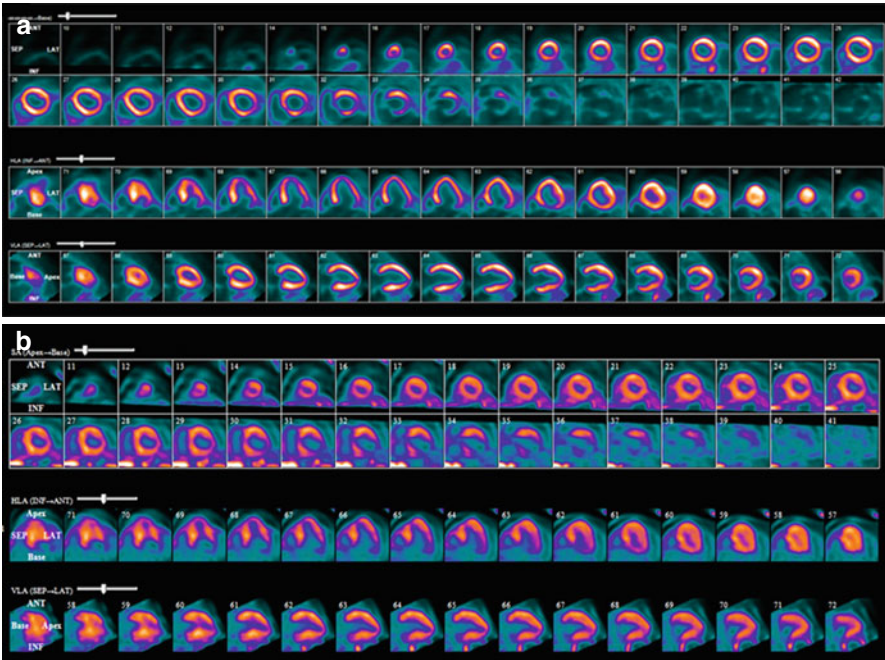


Fig. 5.5 Imaging cardiac amyloidosis with PET radiotracers. F-18 florbetapir PET in a 65-year-old man with light chain cardiac amyloidosis (**a**) and in a 72-year-old man with transthyretin cardiac amyloidosis (**b**). The short-axis (*top*), vertical long-axis (*middle*), and horizontal long-axis (*bottom*) images demonstrate intense and diffusely increased radiotracer uptake in the left and right ventricles

Increased myocardial Tc-99m DPD uptake is directly related to myocardial amyloid burden; it correlates linearly with LV mass on echocardiography [45] and to prolongation of myocardial T-1 relaxation times (CMR), markers of amyloid burden [38]. Furthermore, in 63 patients with hereditary ATTR cardiac amyloidosis, increased heart-to-whole body ratio in conjunction with increased wall thickness was associated with a higher risk of major adverse cardiovascular events [48]. Notably, unlike echocardiography and CMR, Tc-99m PYP or DPD cannot be used as screening test for cardiac amyloidosis—a negative PYP study does not rule out AL cardiac amyloidosis [9]. To address that, a number of amyloid-binding SPECT radiotracers as well as neuronal imaging agents have been tested.

5.3 Imaging Cardiac Sympathetic Denervation with I-123 MIBG

Certain forms of familial ATTR amyloidoses predominantly affect the nervous system with or without concomitant cardiac involvement [3]. A SPECT radiotracer I-123mIBG is a norepinephrine analog that has been successfully used to directly image cardiac adrenergic innervation [49]. Myocardial denervation identified by

I-123 mIBG imaging is an early marker of cardiac amyloidosis in individuals with familial amyloid polyneuropathy (ATTRm) [50] [51] as well as in AL amyloidosis [52]. Delahaye et al. [50] studied 17 patients with biopsy-proven familial amyloid polyneuropathy and found that cardiac I-123 mIBG uptake was significantly decreased in familial amyloid polyneuropathy patients, with no difference in wash-out rates despite preserved left ventricular systolic function and cardiac perfusion. Imaging myocardial denervation, however, remains an indirect method to image early familial cardiac amyloidosis. Therefore, more recently, the focus has shifted to the use of SPECT bone imaging agents to amyloid-binding SPECT and PET agents to identify early cardiac amyloidosis.

5.4 Amyloid-Binding SPECT Radiotracers

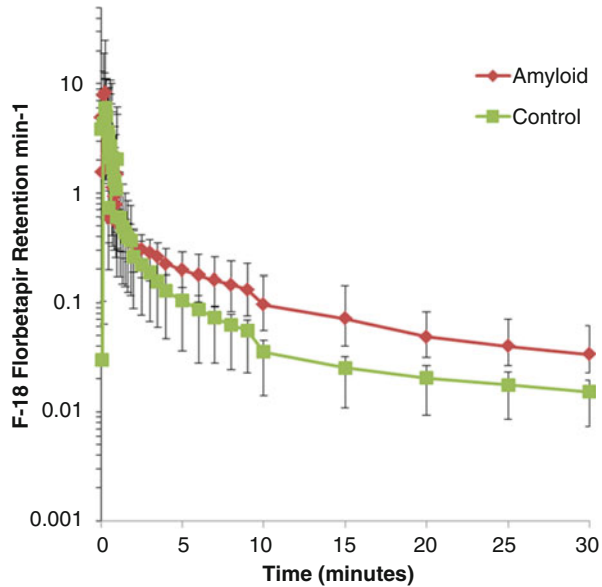
I-123-labeled serum amyloid P component, SAP [53], and Tc-99m-labeled aprotinin [54, 55], are amyloid-binding SPECT tracers. I-123 SAP binds to amyloid fibrils irrespective of precursor protein and can quantify whole-body amyloid load in individuals with systemic AL amyloidosis [53]. But, it has limited availability and a limited signal-to-noise ratio which precludes its use for cardiac imaging [53]. Clinical experience with Tc-99m-labeled aprotinin is more limited, likely due to its limited binding affinity to myocardial amyloid [54, 56, 57]. Furthermore, due to the imaging characteristics, quantitation of radiotracer uptake is challenging with SPECT amyloid radiotracers. This challenge is addressed by the novel amyloid-binding PET radiotracers—C-11 Pittsburgh B compound (PiB), F-18 florbetapir, F-18 florbetaben, and F-18 flutemetamol. Though these radiotracers were originally developed for imaging beta amyloid in the brain, recent pilot studies demonstrate an exciting role for C-11 PiB [58, 59] and F-18 florbetapir [60] for cardiac amyloidosis imaging.

5.5 Amyloid-Binding PET Radiotracers

C-11 Pittsburgh B compound [58, 59] and F-18 florbetapir [60], amyloid-binding PET tracers, appear to nonselectively image AL and ATTR cardiac amyloidosis (Fig. 5.6a, b). In a pilot study of 15 patients (amyloidosis=10 and healthy controls=5), Antoni et al. [46] demonstrated that all patients with cardiac amyloid and none of the healthy control subjects demonstrated myocardial C-11 PiB uptake. The myocardial retention of C-11 PiB was significantly higher in amyloid compared to healthy hearts (0.054/min vs. 0.025/min, $p=0.0007$) [46]. Similar results were demonstrated with F-18 florbetapir, with a significantly higher myocardial retention of F-18 florbetapir by patients with cardiac amyloidosis compared to healthy controls (Fig. 5.6).

F-18 florbetapir myocardial retention index trended higher in patients with AL compared to ATTR cardiac amyloidosis [60]. The median target-to-background (blood pool) ratio of mean SUV (standardized uptake value) was also significantly higher in the amyloid when compared with the control subjects [1.84 (1.64–2.50) vs.

Fig. 5.6 Myocardial retention of F-18 florbetapir in control and amyloid subjects. The mean F-18 florbetapir myocardial retention index was significantly greater in subjects with cardiac amyloidosis (*red line*) compared to control subjects without cardiac amyloidosis (*green line*). The error bars represent the range of values



1.26 (0.91–1.36), $P=0.001$]. Furthermore, in one subject with cardiac AL amyloidosis and the systemic AL amyloidosis in remission, myocardial florbetapir uptake was significantly lower than in individuals with active systemic AL amyloidosis [60]. These findings were confirmed with C-11 PiB imaging in another study of 22 patients with 5 patients who were treated for AL amyloidosis [59]. The maximal myocardial to blood pool target-to-background ratio was significantly higher in amyloidosis patients compared to controls [median 3.86 (range 1.68–19.92) vs. 0.97 (range 0.76–1.23), $p<0.001$]. Notably, five individuals who received chemotherapy for systemic AL amyloidosis demonstrated a significantly lower target-to-background ratio [median 10.39 (range 1.69–19.92) vs. 2.29 (range 1.68–3.81), $p<0.014$]. The results of the three pilot studies together suggest that amyloid imaging with C-11 PiB and F-18 florbetapir may have a potential role for quantitative targeted amyloid imaging. Further studies are warranted to understand if these agents may be helpful to assess myocardial response to anti-amyloid therapy.

Conclusions

Significant developments have expanded our understanding of the pathogenesis, evaluation, and management of patients with cardiac amyloidosis. Several novel therapies are dramatically reducing circulating light chains or transthyretin levels and offer the potential to improve outcomes of individuals with cardiac amyloidosis. However, a clinical diagnosis of cardiac amyloidosis can be challenging. Symptoms are confusing due to systemic illness. Typical low-voltage ECG is neither sensitive nor specific. Echocardiography is typically the initial test in symptomatic individuals. If echocardiography is typical, a histological diagnosis by endomyocardial biopsy (for ATTR) or tissue biopsy (AL) is the next step. Advanced CMR and radionuclide imaging make possible, for

the first time, accurate and quantitative imaging of whole heart amyloid burden. Indeed, but, CMR cannot distinguish AL from ATTR amyloidosis. Cardiac SPECT with bone imaging agents offer a significant advantage in that regard. They specifically identify cardiac ATTR amyloidosis and may mitigate the need for an endomyocardial biopsy in certain individuals. Cardiac SPECT bone imaging agents are sensitive and specific for ATTR cardiac amyloidosis and may mitigate the need for an endomyocardial biopsy in some of these individuals. Future imaging-guided clinical trials will determine whether advances in imaging can aid in the development of novel anti-amyloid therapies that can improve the lives of individuals with this devastating disease.

References

1. Falk RH. Diagnosis and management of the cardiac amyloidoses. *Circulation*. 2005;112:2047–60.
2. Merlini G, Bellotti V. Molecular mechanisms of amyloidosis. *N Engl J Med*. 2003;349:583–96.
3. Ruberg FL, Berk JL. Transthyretin (ttr) cardiac amyloidosis. *Circulation*. 2012;126:1286–300.
4. Quarta CC, Buxbaum JN, Shah AM, Falk RH, Claggett B, Kitzman DW, Mosley TH, Butler KR, Boerwinkle E, Solomon SD. The amyloidogenic v122i transthyretin variant in elderly black americans. *N Engl J Med*. 2015;372:21–9.
5. Dubrey SW, Cha K, Skinner M, LaValley M, Falk RH. Familial and primary (al) cardiac amyloidosis: echocardiographically similar diseases with distinctly different clinical outcomes. *Heart*. 1997;78:74–82.
6. Rapezzi C, Merlini G, Quarta CC, et al. Systemic cardiac amyloidoses: disease profiles and clinical courses of the 3 main types. *Circulation*. 2009;120:1203–12.
7. Merlini G, Wechalekar AD, Palladini G. Systemic light chain amyloidosis: an update for treating physicians. *Blood*. 2013;121:5124–30.
8. Dubrey SW, Davidoff R, Skinner M, Bergethon P, Lewis D, Falk RH. Progression of ventricular wall thickening after liver transplantation for familial amyloidosis. *Transplantation*. 1997;64:74–80.
9. Falk RH, Quarta CC, Dorbala S. How to image cardiac amyloidosis. *Circ Cardiovasc Imaging*. 2014;7:552–62.
10. Rahman JE, Helou EF, Gelzer-Bell R, et al. Noninvasive diagnosis of biopsy-proven cardiac amyloidosis. *J Am Coll Cardiol*. 2004;43:410–5.
11. Murtagh B, Hammill SC, Gertz MA, Kyle RA, Tajik AJ, Grogan M. Electrocardiographic findings in primary systemic amyloidosis and biopsy-proven cardiac involvement. *Am J Cardiol*. 2005;95:535–7.
12. Seward JB, Casacang-Verzosa G. Infiltrative cardiovascular diseases: cardiomyopathies that look alike. *J Am Coll Cardiol*. 2010;55:1769–79.
13. Rapezzi C, Quarta CC, Obici L, et al. Disease profile and differential diagnosis of hereditary transthyretin-related amyloidosis with exclusively cardiac phenotype: an Italian perspective. *Eur Heart J*. 2013;34:520–8.
14. Rapezzi C, Quarta CC, Guidalotti PL, et al. Role of (99m)tc-dpd scintigraphy in diagnosis and prognosis of hereditary transthyretin-related cardiac amyloidosis. *JACC Cardiovasc Imaging*. 2011;4:659–70.
15. Klein AL, Hatle LK, Burstow DJ, et al. Doppler characterization of left ventricular diastolic function in cardiac amyloidosis. *J Am Coll Cardiol*. 1989;13:1017–26.
16. Klein AL, Hatle LK, Burstow DJ, et al. Comprehensive doppler assessment of right ventricular diastolic function in cardiac amyloidosis. *J Am Coll Cardiol*. 1990;15:99–108.

17. Klein AL, Hatle LK, Taliercio CP, et al. Prognostic significance of doppler measures of diastolic function in cardiac amyloidosis. A doppler echocardiography study. *Circulation*. 1991;83:808–16.
18. Klein AL, Hatle LK, Taliercio CP, et al. Serial doppler echocardiographic follow-up of left ventricular diastolic function in cardiac amyloidosis. *J Am Coll Cardiol*. 1990;16:1135–41.
19. Buss SJ, Emami M, Mereles D, et al. Longitudinal left ventricular function for prediction of survival in systemic light-chain amyloidosis: incremental value compared with clinical and biochemical markers. *J Am Coll Cardiol*. 2012;60:1067–76.
20. Koyama J, Ray-Sequin PA, Davidoff R, Falk RH. Usefulness of pulsed tissue doppler imaging for evaluating systolic and diastolic left ventricular function in patients with al (primary) amyloidosis. *Am J Cardiol*. 2002;89:1067–71.
21. Koyama J, Ray-Sequin PA, Falk RH. Prognostic significance of ultrasound myocardial tissue characterization in patients with cardiac amyloidosis. *Circulation*. 2002;106:556–61.
22. Koyama J, Ray-Sequin PA, Falk RH. Longitudinal myocardial function assessed by tissue velocity, strain, and strain rate tissue doppler echocardiography in patients with al (primary) cardiac amyloidosis. *Circulation*. 2003;107:2446–52.
23. Ogiwara F, Koyama J, Ikeda S, Kinoshita O, Falk RH. Comparison of the strain doppler echocardiographic features of familial amyloid polyneuropathy (fap) and light-chain amyloidosis. *Am J Cardiol*. 2005;95:538–40.
24. Siqueira-Filho AG, Cunha CL, Tajik AJ, Seward JB, Schattenberg TT, Giuliani ER. M-mode and two-dimensional echocardiographic features in cardiac amyloidosis. *Circulation*. 1981;63:188–96.
25. Carroll JD, Gaasch WH, McAdam KP. Amyloid cardiomyopathy: characterization by a distinctive voltage/mass relation. *Am J Cardiol*. 1982;49:9–13.
26. Nagueh SF, Appleton CP, Gillebert TC, et al. Recommendations for the evaluation of left ventricular diastolic function by echocardiography. *J Am Soc Echocardiogr*. 2009;22:107–33.
27. Cappelli F, Porciani MC, Bergesio F, et al. Right ventricular function in al amyloidosis: characteristics and prognostic implication. *Eur Heart J Cardiovasc Imaging*. 2012;13:416–22.
28. Baccouche H, Maunz M, Beck T, et al. Differentiating cardiac amyloidosis and hypertrophic cardiomyopathy by use of three-dimensional speckle tracking echocardiography. *Echocardiography*. 2012;29:668–77.
29. Phelan D, Collier P, Thavendiranathan P, et al. Relative apical sparing of longitudinal strain using two-dimensional speckle-tracking echocardiography is both sensitive and specific for the diagnosis of cardiac amyloidosis. *Heart*. 2012;98:1442–8.
30. Bellavia D, Pellikka PA, Dispenzieri A, et al. Comparison of right ventricular longitudinal strain imaging, tricuspid annular plane systolic excursion, and cardiac biomarkers for early diagnosis of cardiac involvement and risk stratification in primary systematic (al) amyloidosis: a 5-year cohort study. *Eur Heart J Cardiovasc Imaging*. 2012;13:680–9.
31. Fattori R, Rocchi G, Celletti F, Bertaccini P, Rapezzi C, Gavelli G. Contribution of magnetic resonance imaging in the differential diagnosis of cardiac amyloidosis and symmetric hypertrophic cardiomyopathy. *Am Heart J*. 1998;136:824–30.
32. Maceira AM, Joshi J, Prasad SK, et al. Cardiovascular magnetic resonance in cardiac amyloidosis. *Circulation*. 2005;111:186–93.
33. Syed IS, Glockner JF, Feng D, et al. Role of cardiac magnetic resonance imaging in the detection of cardiac amyloidosis. *JACC Cardiovasc Imaging*. 2010;3:155–64.
34. Vogelsberg H, Mahrholdt H, Deluigi CC, et al. Cardiovascular magnetic resonance in clinically suspected cardiac amyloidosis: noninvasive imaging compared to endomyocardial biopsy. *J Am Coll Cardiol*. 2008;51:1022–30.
35. Austin BA, Tang WH, Rodriguez ER, et al. Delayed hyper-enhancement magnetic resonance imaging provides incremental diagnostic and prognostic utility in suspected cardiac amyloidosis. *JACC Cardiovasc Imaging*. 2009;2:1369–77.
36. White JA, Kim HW, Shah D, et al. CMR imaging with rapid visual t1 assessment predicts mortality in patients suspected of cardiac amyloidosis. *JACC Cardiovasc Imaging*. 2014;7:143–56.
37. Karamitsos TD, Piechnik SK, Banyersad SM, et al. Noncontrast t1 mapping for the diagnosis of cardiac amyloidosis. *JACC Cardiovasc Imaging*. 2013;6:488–97.

38. Fontana M, Banypersad SM, Treibel TA, et al. Native T1 mapping in transthyretin amyloidosis. *JACC Cardiovasc Imaging*. 2014;7:157–65.
39. Banypersad SM, Fontana M, Maestrini V, et al. T1 mapping and survival in systemic light-chain amyloidosis. *Eur Heart J*. 2014;36(4):244–51.
40. Fontana M, Chung R, Hawkins PN, Moon JC. Cardiovascular magnetic resonance for amyloidosis. *Heart Fail Rev*. 2015;20(2):133–44.
41. Banypersad SM, Sado DM, Flett AS, et al. Quantification of myocardial extracellular volume fraction in systemic al amyloidosis: an equilibrium contrast cardiovascular magnetic resonance study. *Circ Cardiovasc Imaging*. 2013;6:34–9.
42. Mongeon FP, Jerosch-Herold M, Coelho-Filho OR, Blankstein R, Falk RH, Kwong RY. Quantification of extracellular matrix expansion by cmr in infiltrative heart disease. *JACC Cardiovasc Imaging*. 2012;5:897–907.
43. Falk RH, Lee VW, Rubinow A, Hood Jr WB, Cohen AS. Sensitivity of technetium-99m-pyrophosphate scintigraphy in diagnosing cardiac amyloidosis. *Am J Cardiol*. 1983;51:826–30.
44. Perugini E, Guidalotti PL, Salvi F, et al. Noninvasive etiologic diagnosis of cardiac amyloidosis using 99mTc-3,3-diphosphono-1,2-propanodicarboxylic acid scintigraphy. *J Am Coll Cardiol*. 2005;46:1076–84.
45. Rapezzi C, Quarta CC, Guidalotti PL, et al. Usefulness and limitations of 99mTc-3,3-diphosphono-1,2-propanodicarboxylic acid scintigraphy in the aetiological diagnosis of amyloidotic cardiomyopathy. *Eur J Nucl Med Mol Imaging*. 2011;38:470–8.
46. Bokhari S, Castano A, Pozniakoff T, Deslisle S, Latif F, Maurer MS. (99m)Tc-pyrophosphate scintigraphy for differentiating light-chain cardiac amyloidosis from the transthyretin-related familial and senile cardiac amyloidoses. *Circ Cardiovasc Imaging*. 2013;6:195–201.
47. Hutt DF, Quigley AM, Page J, et al. Utility and limitations of 3,3-diphosphono-1,2-propanodicarboxylic acid scintigraphy in systemic amyloidosis. *Eur Heart J Cardiovasc Imaging*. 2014;15:1289–98.
48. Rapezzi C, Guidalotti P, Salvi F, Riva L, Perugini E. Usefulness of 99mTc-dpd scintigraphy in cardiac amyloidosis. *J Am Coll Cardiol*. 2008;51:1509–10.
49. Travin MI. Cardiac autonomic imaging with SPECT tracers. *J Nucl Cardiol*. 2013;20:128–43.
50. Delahaye N, Dinanian S, Slama MS, et al. Cardiac sympathetic denervation in familial amyloid polyneuropathy assessed by iodine-123 metaiodobenzylguanidine scintigraphy and heart rate variability. *Eur J Nucl Med*. 1999;26:416–24.
51. Noordzij W, Glaudemans AW, van Rheenen RW, et al. (123)I-labelled metaiodobenzylguanidine for the evaluation of cardiac sympathetic denervation in early stage amyloidosis. *Eur J Nucl Med Mol Imaging*. 2012;39:1609–17.
52. Hongo M, Urushibata K, Kai R, et al. Iodine-123 metaiodobenzylguanidine scintigraphic analysis of myocardial sympathetic innervation in patients with AL (primary) amyloidosis. *Am Heart J*. 2002;144:122–9.
53. Hawkins PN, Lavender JP, Pepys MB. Evaluation of systemic amyloidosis by scintigraphy with 123I-labeled serum amyloid P component. *N Engl J Med*. 1990;323:508–13.
54. Aprile C, Marinone G, Saponaro R, Bonino C, Merlini G. Cardiac and pleuropulmonary AL amyloid imaging with technetium-99m labelled aprotinin. *Eur J Nucl Med*. 1995;22:1393–401.
55. Han S, Chong V, Murray T, et al. Preliminary experience of 99mTc-aprotinin scintigraphy in amyloidosis. *Eur J Haematol*. 2007;79:494–500.
56. Cardoso I, Pereira PJ, Damas AM, Saraiva MJ. Aprotinin binding to amyloid fibrils. *Eur J Biochem*. 2000;267:2307–11.
57. Minamoto R, Kubota K, Ishii K, et al. Re-evaluating the potentials and limitations of (99m)Tc-aprotinin scintigraphy for amyloid imaging. *Am J Nucl Med Mol Imaging*. 2013;3:261–71.
58. Antoni G, Lubberink M, Estrada S, et al. In vivo visualization of amyloid deposits in the heart with 11C-pib and PET. *J Nucl Med*. 2013;54:213–20.
59. Lee SP, Lee ES, Choi H, et al. (11)C-pittsburgh b PET imaging in cardiac amyloidosis. *JACC Cardiovasc Imaging*. 2015;8:50–9.
60. Dorbala S, Vangala D, Semer J, et al. Imaging cardiac amyloidosis: a pilot study using (18)F-florbetapir positron emission tomography. *Eur J Nucl Med Mol Imaging*. 2014;41:1652–62.